2013 IEEE International Conference on Robotics and Automation (ICRA)
Karlsruhe, Germany, May 6-10, 2013

Torque Estimation Technique of Robotic Joint with Harmonic Drive Transmission

Hongwei Zhang, Saleh Ahmad, and Guangjun Liu, *Senior Member*, *IEEE*

***Abstract*— A joint torque estimation technique utilizing the existing structural elasticity of robotic joints with harmonic drive transmission is proposed in this paper. Joint torque sensing is one of the key techniques for achieving high-performance robot control, especially for robots working in unstructured environments. The proposed joint torque estimation technique uses link-side position measurement along with a proposed harmonic derive model to realize stiff and sensitive torque estimation. The proposed joint torque estimation method has been experimentally studied in comparison with a commercial torque sensor, and the results have attested the effectiveness of the proposed torque estimation technique.**

I. INTRODUCTION

Harmonic drives, invented in the 1950s [1], are widely used in robotic systems, due to their desirable features of near-zero backlash, compactness, light weight, high torque capacity, high gear ratio and coaxial assembly. These distinctive characteristics of harmonic drives vindicate their widespread applications, especially in electrically-driven robot manipulators.

Joint torque feedback (JTF) has been widely recognized to improve the performance of robot control in the robotics community [2], [3], [4], [5]. The JTF is generally used in motion control of robot manipulators to suppress the effect of load torques [6]. In addition, joint torque sensors can considerably ease the necessity to model the link dynamics. Therefore, JTF can be used in the dynamic control of robots without the need of computing the robot inverse dynamics. Joint torque sensing is also valuable in force, compliance, and impedance control. In addition, joint torque sensing is necessary for collision detection and reaction.

Measurement or estimation of the torque transmitted by the harmonic drive transmission is required for the implementation of JTF control methods. Conventionally, to implement such control strategies, the robot is equipped with joint torque sensors or a multi-axis force/torque (F/T) sensor. When using F/T sensor at the robot wrist, the estimation of joint torques requires additional calculations, and the results may be affected by computation delays and model errors [7]. Furthermore, the commercially available F/T sensors are costly and require additional space and mechanical modification to the joints.

This work is supported in part by the Natural Sciences and Engineering Research Council (NSERC) of Canada, and in part by the Canada Research Chair program.

The authors are with the Department of Aerospace Engineering, Ryerson University, 350 Victoria Street, Toronto, Ontario, Canada M5B 2K3. (G. Liu is the corresponding author. Phone: 416-979-5000; email: gjliu@ryerson.ca)

There are several techniques of direct joint torque sensing, e.g., joint torque sensors based on elastic elements that are positioned at the output of each joint of the robot [8], [9]. However, these additional compliant elements may compromise the joint stiffness, especially for robotic joints with harmonic drive transmission because of the already existed elasticity of the flexspline. Vischer et al. [8] and Tsetserukou et al. [9] measure deformation of an elastic body after the reduction mechanism with optical distance sensors. Kawakami et al. [10] used a linear encoder to measure the torsional deformation of the additional elastic body. Low sensor stiffness is unavoidable in the case when high measurement resolution is required. This is due to the fact that measurement accuracy is inversely proportional to the sensor stiffness. Low sensor stiffness is undesirable as it usually results in complicated joint dynamics. The additional elastic component also affects the link position measurement accuracy.

Another joint torque sensing technique is based on the method proposed by Hashimoto et al. in [11]. Joint torque sensing is achieved by mounting strain gages directly on the harmonic derive, which is usually referred to as built-in torque sensing [11], [12], [13]. In this technique, the torsional compliance of harmonic drives is utilized for torque sensing. A drawback of this technique is that the elliptical shape of the wave generator in harmonic drive transmissions introduces local torque ripple that is dependent on the position of the flexspline. It is difficult to separate the torque signal from the local torque ripple when the applied torque is sensed at the flexspline [14]. Also, torque sensors based on strain gages that are directly cemented on the flexspline require regular maintenance and tuning.

Recently, high resolution absolute position encoders become commercially available. This makes it possible to measure the torsional deformation of harmonic drive. In this paper, we develop a joint torque estimation method based on a proposed harmonic drive compliance model. The torsional deformation of the harmonic drive is measured using link-side encoder and the resulted measurement is used with the proposed harmonic drive compliance model to estimate the joint torque. The proposed torque estimation method is economical and represents an effective way of torque estimation for robots with harmonic drives.

This paper is organized into four sections as follows: the harmonic drive kinematic model, compliance model, and the torque estimation algorithm are presented in Section II. Experimental setup and results are given and discussed in Section III, and concluding remarks are in Section IV.

978-1-4673-5643-5/13/$31.00 ©2013 IEEE

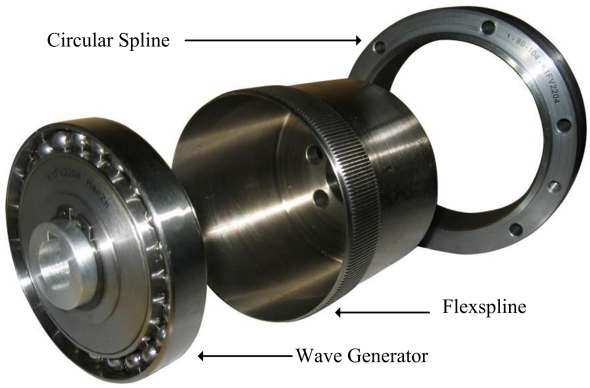

Fig. 1. Exploded view of a harmonic drive showing the three components.

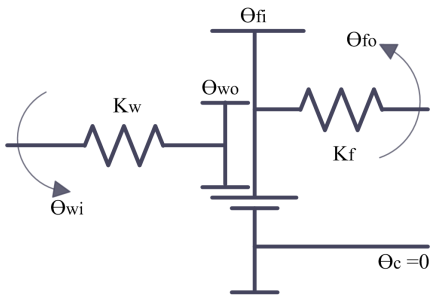

Fig. 2. Kinematic representation of a harmonic drive showing the three ports.

II. TORQUE ESTIMATION TECHNIQUE

A typical harmonic drive consists of three main components as shown in Fig. 1. The wave generator (WG) is connected to the motor shaft, the circular spline (CS) is connected to the joint housing, and the flexspline (FS) is sandwiched in between (CS and WG) and connected to the joint output. The WG consists of an elliptical disk (rigid elliptical inner-race), called wave generator plug, and an outer ball bearing both of which are separate parts. The wave generator plug is inserted into the bearing, thereby giving the bearing an elliptical shape as well. The FS fits tightly over WG; when the WG plug is rotated, the FS deforms and molds into the shape of the rotating ellipse but does not rotate with WG.

In order to estimate the joint torque based on position measurements, a compliance model of the harmonic drive is required. In this section, a new harmonic drive compliance model is presented and used in the proposed joint torque estimation technique. The rest of this section is organized as follows: the kinematic relationship between the angular positions at the harmonic drive components are described first, the proposed harmonic drive compliance model is described next, and finally, the proposed joint torque estimation method is presented.

A. Harmonic Drive Kinematic Model

Typically, for robotic joints with harmonic drive transmission, the circular spline is usually fixed leaving the wave generator and flexspline for input and output. The input/ouput kinematic relationship, as explained in [15], equates the angular positions at the components of the harmonic drive:

$$\theta_w = N\theta_f \tag{1}$$

where θ_w is the wave generater position, θ_f is the flexspline output position, and N is the gear ratio. The static force balance can be described as

$$T_w = \frac{1}{N}T_f \tag{2}$$

where T_w is the torque at wave generater and T_f is the flexspline output torque. Equations (1) and (2) represent the harmonic drive's ideal linear input/output relationship, and the harmonic drive transmission is treated as a perfectly rigid gear reduction mechanism. However, the empirical measurements of the input/output relationship provided in the cited literature clearly show that the output is not linearly related to the input [16]. The causes of this nonlinearity are torsional compliance in the harmonic drive components, nonlinear viscous friction, and the kinematic error due to gear meshing, which takes a more comprehensive harmonic drive model to incorporate. The kinematic error, Θ_{err} can be defined as

$$\Theta_{err} = \theta_{fi} - \frac{\theta_{wo}}{N} \tag{3}$$

It is well known that harmonic drives suffer nonlinear friction torque. Considering friction, Equation (2) becomes

$$T_w = \frac{1}{N}(T_F - T_{Fr}) \tag{4}$$

where T_{Fr} is the harmonic drive friction torque.

The harmonic drive torsional compliance is due to flexibilities in both flexspline and wave generator [17]. Considering the flexibility of flexspline and wave generator, a kinematic representation of a harmonic drive is illustrated in Fig. 2.

The torsional angle of the flexspline can be defined as

$$\triangle\theta_f = \theta_{fo} - \theta_{fi} \tag{5}$$

where θ_{fi} denotes the angular position at the flexspline gear-side (gear-toothed circumference), θ_{fo} denotes the flexspline angular position at the load side which is measured using the link-side encoder. Let the wave generator torsional angle be defined as

$$\triangle\theta_w = \theta_{wo} - \theta_{wi} \tag{6}$$

where θ_{wo}, θ_{wi} denote the positions of the wave generator outside part (ball bearing outer rim) and the center part (wave generator plug), respectively. Note that, θ_{fi} and θ_{wo} are not available as only θ_{fo} and θ_{wi} are measured by the link-side encoder and the motor-side encoder, respectively.

The total torsional angle of the harmonic drive can be written as

$$\triangle\theta = \theta_{fo} - \frac{\theta_{wi}}{N} \tag{7}$$

Substituting (3), (5) and (6) into (7), yields

$$\triangle\theta = \triangle\theta_f + \frac{\triangle\theta_w}{N} + \Theta_{err} \tag{8}$$

To determine the kinematic error, Θ_{err}, the joint is rotated clockwise and counterclockwise one complete output revolution with no payload. The total torsional deformation $\triangle\theta_{cw}$ and $\triangle\theta_{ccw}$ are measured during this process.

$$\triangle\theta_{cw} = \triangle\theta_f + \frac{\triangle\theta_{w_{cw}}}{N} + \Theta_{err}$$

$$\triangle\theta_{ccw} = \triangle\theta_f + \frac{\triangle\theta_{w_{ccw}}}{N} + \Theta_{err}$$

where $\triangle\theta_{w_{cw}}$ and $\triangle\theta_{w_{ccw}}$ are the wave generator torsional deformation in the clockwise and counterclockwise direction, respectively.

Because the output torque is equal to zero, the flexspline torsional deformation is also equal to zero, $\triangle\theta_f = 0$. Assuming that the torsional deformation of the wave generator is symmetric, for example

$$\triangle\theta_{w_{cw}} = -\triangle\theta_{w_{ccw}}$$

Then, the kinematic error can be determined from the following expression

$$\Theta_{err} = (\triangle\theta_{cw} + \triangle\theta_{ccw})/2$$

B. Harmonic Drive Compliance Model

A typical harmonic drive stiffness curve is shown in Fig. 3, which features increasing stiffness with displacement and hysteresis behavior. As described above, the total harmonic drive torsional deformation comprises deformation of both the flexspline and the wave generator. A model of the compliance of each harmonic drive component is presented in the following.

Based on the curve shown in Fig. 3 and experimental observation, the harmonic drive torsional deformation is largely contributed by the flexspline torsional compliance. The flexspline torsional compliance is described in [15], where $\triangle\theta_f$ is approximated by a piecewise linear function of the output torque, see Fig. 3.

$$\triangle\theta_f = \begin{cases} \frac{T_f}{K_1} & T_f \le T_1 \\ \frac{T_1}{K_1} + \frac{(T_f - T_1)}{K_2} & T_1 < T_f < T_2 \\ \frac{T_1}{K_1} + \frac{(T_2 - T_1)}{K_2} + \frac{(T_f - T_2)}{K_3} & T_f \ge T_2 \end{cases} \quad (9)$$

where K_1, K_2, K_3, T_1, and T_2 are given by the manufacture. The slope of the curve shown in Fig. 3 determines the harmonic drive stiffness. For simplicity, the curve is approximated by three straight-line segments with stiffness of K_1, K_2, and K_3. Stiffness K_1 applies for flexspline torque of 0 to T_1. Stiffness K_3 applies for flexspline torque greater than T_2. Stiffness K_2 applies for flexspline ranging from T_1 to T_2.

It is well known that harmonic drives suffer from both nonlinear torsional compliance and hysteresis behavior. We assume that hysteresis is caused by the compliance of the wave generator and the harmonic drive friction. When the wave generator's torque (torque applied by the motor) is within harmonic drive's starting torque, the harmonic drive's output torque will not change. Therefore, the harmonic drive torsional deformation can be from $-\Psi/2$ to $\Psi/2$ at zero

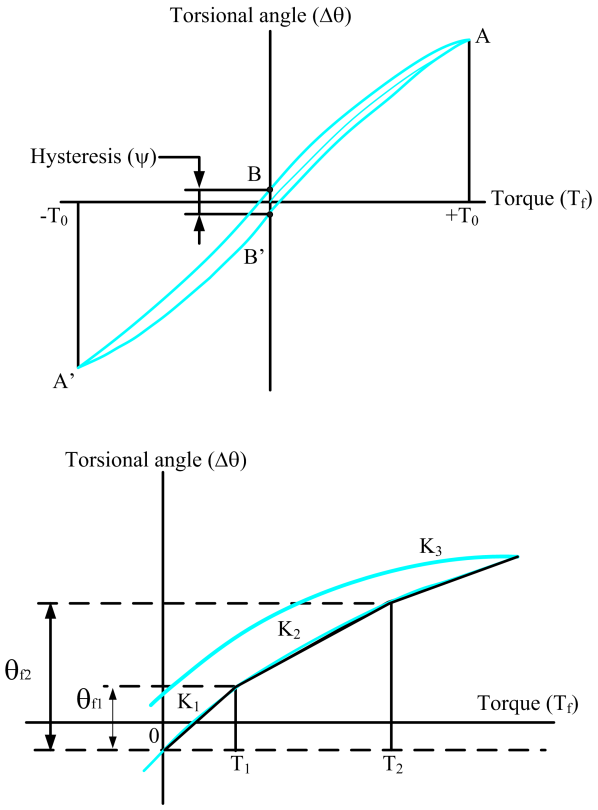

Fig. 3. Typical stiffness and hysteresis curve of a harmonic drive.

torque output. This deformation range decreases to zero sharply at rated torque, which means that the stiffness of wave generator increases sharply. Therefore, to replicate the hysteresis shape of this stiffness curve, the wave generator local elastic coefficient is model as

$$K_w = K_{w0} e^{C_w |T_w|} \quad (10)$$

where K_{w0} and C_w are constants to be determined.

The wave generator torsional angle can be calculated using the following relation

$$\triangle\theta_w = \int_0^{T_w} \frac{d_{T_w}}{K_w} \quad (11)$$

Substituting (10) into (11), we obtain

$$\triangle\theta_w = \frac{sign\,(T_w)}{C_w K_{w0}} \left(1 - e^{-C_w |T_w|}\right) \quad (12)$$

C. Torque Estimation

The total torsional deformation of the harmonic drive is measured using both link-side and motor-side encoders. The wave generator torque T_w is approximated by the motor torque command.

Combining (12) and (8) yields

$$\triangle\theta_f = \triangle\theta - \frac{sign\,(T_w)}{C_w N K_{w0}} \left(1 - e^{-C_w |T_w|}\right) - \Theta_{err} \quad (13)$$

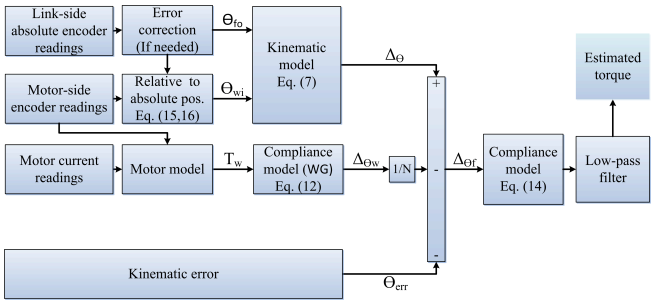

Fig. 4. Block diagram of the proposed torque estimation technique.

Having the flexspline torsional deformation, $\triangle\theta_f$, the joint torque estimate is obtained using the inverse of (9).

$$T_f = \begin{cases} K_1 \triangle\theta_f & \triangle\theta_f \leq \theta_{f1} \\ T_1 + K_2(\triangle\theta_f - \theta_{f1}) & \theta_{f1} < \triangle\theta_f < \theta_{f2} \\ T_2 + K_3(\triangle\theta_f - \theta_{f2}) & \triangle\theta_f \geq \theta_{f2} \end{cases} \quad (14)$$

where $\theta_{f1} = T_1/K_1$ and $\theta_{f2} = T_1/K_1 + (T_2 - T_1)/K_2$.

A block diagram illustrating the proposed torque estimation method is portrayed in Fig. 4.

III. EXPERIMENTAL SETUP AND RESULTS

To verify the proposed torque estimation method, a test station is set up as shown in Fig. 5. The base joint (joint 1) in Fig. 5(c) is developed in our laboratory to investigate the performance of the proposed joint torque estimation method. Joint 2, joint 3, and the link are used as payload. In this experimental setup, the harmonic drive of joint 1 is driven by a brushed DC motor from Maxon, model 218014. A linear power amplifier and the Q8 data acquisition board from Quanser Inc. are used to drive the motor and collect experimental data. The harmonic drive in the setup is SHD-17-100-2SH with gear ratio of 100:1, and rated torque of $16\,Nm$ from Harmonic Drive AG. The link-side position is measured using Netzer absolute position electric encoder (DS-90) with 19-bit resolution and the link-side torque is measured using ATI six-axis F/T sensor, Mini45-ERA. A cross-sectional view of the developed robotic joint with link-side encoder is shown Fig. 5(b). The coefficients used with the harmonic drive compliance model and the physical parameters of the experimental setup are giving in Table I. Robotic joints are usually equipped with optical incremental encoder to measure the motor-side position for control purposes. However, incremental encoders only provide the relative position of the motor shaft. Therefore, a method of calculating the absolute position of the motor shaft is necessary. To obtain the motor absolute position, the joint is rotated 360^0 clockwise free-run while recording the flexspline output position at each encountered index of the incremental encoder, $\theta_{fo}^{cw_i}$. Then the joint is rotated 360^0 counterclockwise, and the flexspline output position (the link-side absolute encoder readings) at each index $\theta_{fo}^{ccw_i}$ is recorded. The offset of the incremental encoder installed at

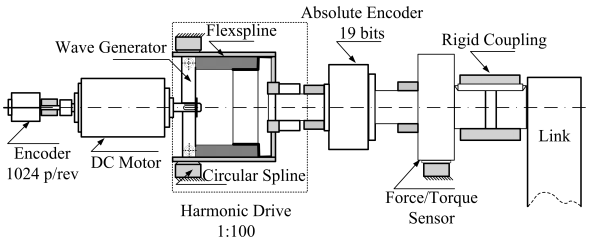

(a)

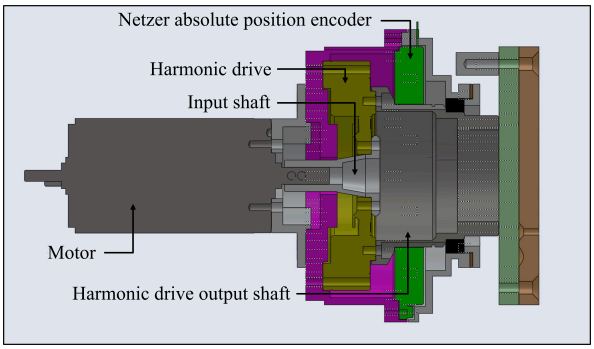

(b)

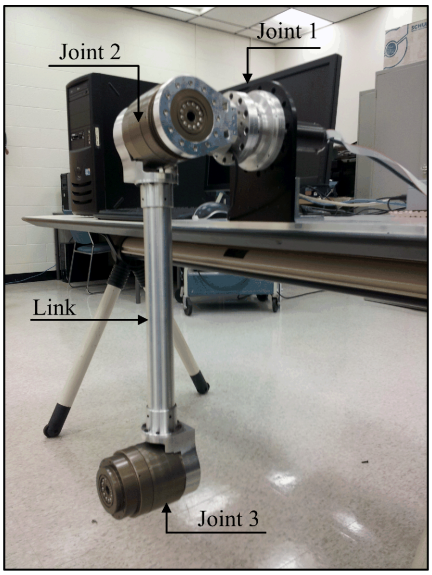

(c)

Fig. 5. Experimental setup. (a) Schematic diagram, (B) Cross-sectional view of the robotic joint with link-side encoder, and (c) Picture of the experimental test setup.

motor-side is determined as

$$\theta_{offset} = \left(\sum_{i=0}^{N-1} \frac{(\theta_{fo}^{cw_i} + \theta_{fo}^{ccw_i} - 2iN/360)}{2}\right)/N \quad (15)$$

where θ_{offset} is the offset between the link-side absolute position measurement and the motor-side incremental encoder relative position measurement.

The absolute position of the motor shaft is estimated using the recorded link-side positions, θ_{fo_0}, at the first encountered

TABLE I

PARAMETERS OF THE EXPERIMENTAL SETUP

Parameter		Joint 1
Harmonic drive compliance model parameters		
K_{w0}	$(N.m/rad)$	1.33
C_w	$(N.m^{-1})$	83.5
K_1	$(N.m/rad)$	8.4×10^3
K_2	$(N.m/rad)$	9.4×10^3
K_3	$(N.m/rad)$	13×10^3
T_1	$(N.m)$	3.9
T_2	$(N.m)$	12
Physical parameters of the experimental setup		
Rotor inertia for joint 1	$(kg.m^2)$	0.114×10^{-4}
Link mass	(kg)	0.641
Link length	(m)	0.45
Mass of joint 1 and 2	(kg)	1.2

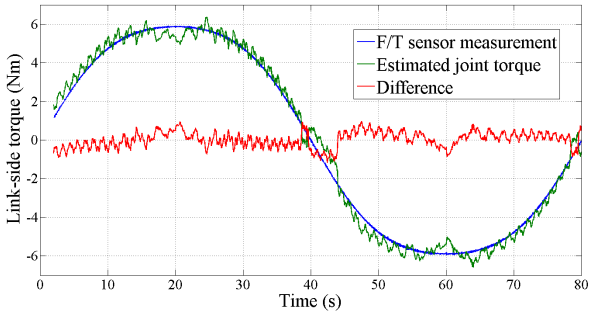

Fig. 6. Estimated torque versus torque measured by F/T sensor (response to slow changes).

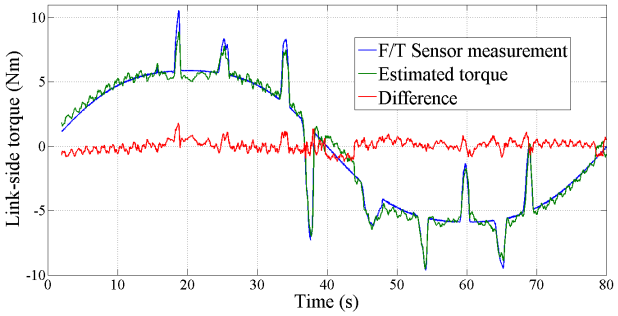

Fig. 7. Estimated torque versus torque measured by F/T sensor (response to fast changes).

index after power-on, as

$$\theta_{wi} = \theta_{offset} + \text{int}(N\theta_{fo_0}/360)\frac{360}{N} + \theta_{IE} \qquad (16)$$

where θ_{IE} is the incremental encoder reading, and int(.) is a conversion function that converts to integer data type.

The efficiency of the proposed torque estimation method is verified by comparing the estimated joint torque to a torque measurement from the ATI F/T sensor mounted on the output of the base joint. Three experiments were conducted to demonstration the effectiveness of the proposed torque estimation method, in which slow, fast, and sudden changes of the load were applied. The results of these experiments are depicted in Fig. 6, Fig. 7, and Fig. 8, respectively. Slow changes of the load torque were introduced by controlling the

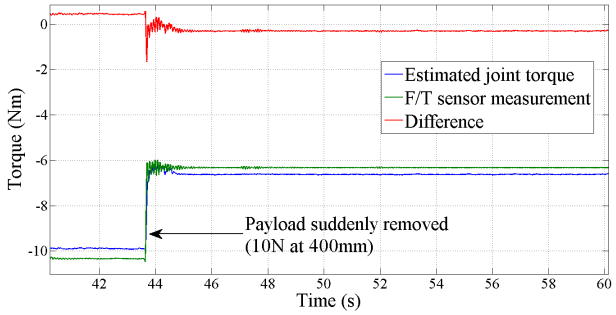

Fig. 8. Estimated torque versus torque measured by F/T sensor (response to sudden payload changes).

joint motion with a sinusoidal desired trajectory. The moving links and joints attached to the base joint introduce the gradually changing load torque. To introduce fast changes to the load torque, external torque was applied manually in both directions. The response of the proposed torque estimation method to sudden changes to the payload was verified by removing a 10 N weight that was initially attached to the link by a wire at a distance of 400 mm from the first joint axis of rotation. During this experiment the joint is controlled to keep its position constant and the load was released suddenly by cutting the wire. The error in torque estimation is around 1 Nm, which is comparable with the commercial F/T sensor.

A. Motion Control with JTF

To demonstrate the efficiency of the proposed torque estimation method, motion control with joint torque feedback was implemented using the experimental setup show in Fig. 5(c). The distributed control method based on joint torque feedback proposed in [3] is adopted in this paper as an application to demonstration the effectiveness of the proposed joint torque estimation method. The results of the this experiment are presented in Fig. 9 and Fig. 10. Fig. 9 shows the desired position while the position error is shown in Fig. 10. In the first 20s of the experiment time, the joint torque feedback was set to zero and the link-side position error is shown in the aria labeled (A) in Fig. 10, the link-side position error when using JTF from F/T sensor is shown in aria labeled (B), and the position error when using JTF with the estimated torque based on the proposed method is shown in aria labeled (C).

B. Passive Control

As another application of joint torque feedback JTF, a simple passive mode controller is implemented. The control law used in the passive mode control is described as

$$\tau = K\,\tau_s \qquad (17)$$

where τ denotes the motor torque command, K is a positive gain, and τ_s is the torque mapped from the joint torque. The estimated joint torque as well as the F/T sensor measurements are used as JTF to the passive mode control and the results are shown in Fig. 11. The joint was Back-driven without joint torque feedback in the area labeled (A) in

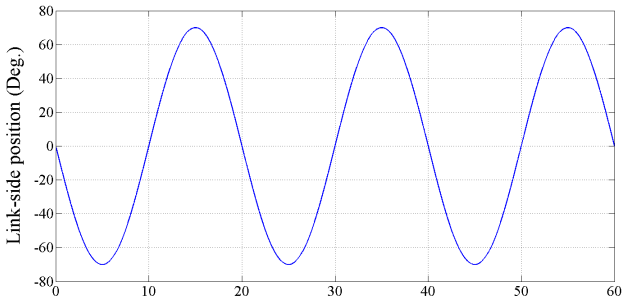

Fig. 9. Desired trajectory for active mode control.

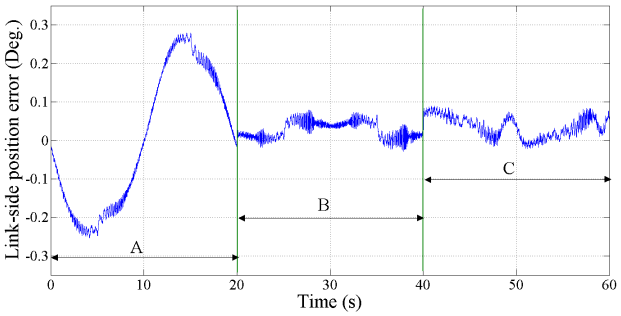

Fig. 10. Active mode experimental results.

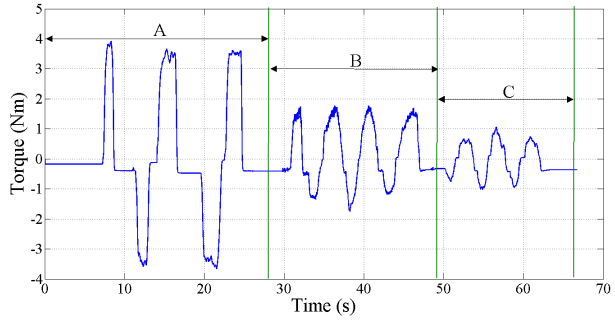

Fig. 11. Passive mode experimental results.

Fig. 11, joint torque feedback with the estimated torque is shown in the area labeled (B), and joint torque feedback with F/T sensor is shown in the area labeled (C). The joint angular position is shown in Fig. 12.

IV. CONCLUSIONS

In this paper, a joint torque estimation method based on position measurement is presented along with a new harmonic drive compliance model. Torque estimation based on position measurements provides an advantage of noise immunity to the estimated joint torque. Using the torsional compliance of harmonic drives instead of an additional elastic component does not change the joint dynamics. Moreover, adding a link-side position sensor has potential to improve joint control accuracy and reduce the cost of joint torque sensing. The estimated torque can be used in robotic control algorithms with JTF and in collision detection/avoidance schemes.

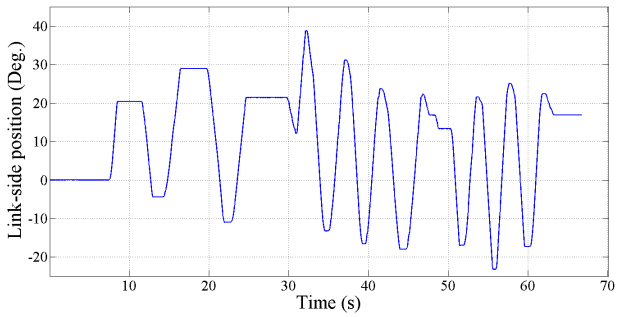

Fig. 12. Measured joint position for passive mode control.

REFERENCES

[1] C. W. Musser, "Strain wave gearing," Patent US 2 906 143, 1955.

[2] F. Aghili, M. Buehler, and J. M. Hollerbach, "Motion control systems with h-infinity positive joint torque feedback," *IEEE Trans. Control Syst. Technol.*, vol. 9, no. 5, pp. 685–695, Sep. 2001.

[3] G. Liu, S. Abdul, and A. Goldenberg, "Distributed modular and reconfigurable robot control with torque sensing," in *Proc. IEEE Int. Conf. on Mechatron. and Autom.*, Jun. 2006, pp. 384–389.

[4] W.-H. Zhu, E. Dupuis, and M. Doyon, "Adaptive control of harmonic drives," *ASME Trans. on Dyn. Syst., Measur., and Contr.*, vol. 129, no. 2, pp. 182–193, Aug. 2007.

[5] L. L. Tien, A. Albu-Schaffer, A. D. Luca, and G. Hirzinger, "Friction observer and compensation for control of robots with joint torque measurement," in *Proc. IEEE/RSJ Int. Conf. on Intel. Robot. and Sys.*, Sep. 2008, pp. 3789–3795.

[6] F. Aghili, J. Hollerbach, and M. Buehler, "A modular and high-precision motion control system with an integrated motor," *IEEE/ASME Trans. on Mech.*, vol. 12, no. 3, pp. 317–329, Jun. 2007.

[7] M. Randazzo, M. Fumagalli, F. Nori, L. Natale, G. Metta, and G. Sandini, "A comparison between joint level torque sensing and proximal f/t sensor torque estimation: implementation on the icub," in *Proc. IEEE/RSJ Int. Conf. on Intel. Robot. and Sys.*, Sep. 2011, pp. 4161–4167.

[8] D. Vischer and O. Khatib, "Design and development of high-performance torque-controlled joints," *IEEE Trans. on Robot. and Autom.*, vol. 11, no. 4, pp. 537–544, Aug. 1995.

[9] D. Tsetserukou, R. Tadakuma, H. Kajimoto, and S. Tachi, "Optical torque sensors for implementation of local impedance control of the arm of humanoid robot," in *Proc. IEEE Int. Conf. on Robot. and Autom.*, May 2006, pp. 1674–1679.

[10] T. K. K., Ayusawa, H. Kaminaga, and Y. Nakamura, "High-fidelity joint drive system by torque feedback control using high precision linear encoder," in *Proc. IEEE Int. Conf. on Robot. and Autom.*, May 2010, pp. 3904–3909.

[11] M. Hashimoto, Y. Kiyosawa, and R. Paul, "A torque sensing technique for robots with harmonic drives," *IEEE Trans. on Robot. and Autom.*, vol. 9, no. 1, pp. 108–116, Feb. 1993.

[12] H. Taghirad and P. Belanger, "Torque ripple and misalignment torque compensation for the built-in torque sensor of harmonic drive systems," *IEEE Trans. on Instr. and Measur.*, vol. 47, no. 1, Feb. 1998.

[13] I. Godler, M. Horiuchi, M. Hashimoto, and T. Ninomiya, "Accuracy improvement of built-in torque sensing for harmonic drives," *IEEE/ASME Trans. on Mech.*, vol. 5, no. 4, pp. 360–366, Dec. 2000.

[14] J. Sensinger and R. Weir, "Improved torque fidelity in harmonic drive sensors through the union of two existing strategies," *IEEE/ASME Trans. on Mech.*, vol. 11, no. 4, pp. 457–461, Aug. 2006.

[15] H. drive technologies. (2012) Ultra-flat component sets and gearheads. [Online]. Available: http://www.harmonicdrive.net/support/catalogs/

[16] P. Curt, R. J. Thomas, and S. Deming, "A high-fidelity harmonic drive model," *ASME J. of Dyn. Sys., Measur. and Contr.*, vol. 134, no. 1, pp. 457–461, Apr. 2012.

[17] C. Kennedy and J. Desai, "Modeling and control of the mitsubishi pa-10 robot arm harmonic drive system," *IEEE/ASME Trans. on Mech.*, vol. 10, no. 3, pp. 263–274, Jun. 2005.